Switching Off FRET in the Hybrid Assemblies of Diblock Copolymer Micelles, Quantum Dots, and Dyes by Plasmonic Nanoparticles

Ki-Se Kim,[†] Jeong-Hee Kim,[†] Hun Kim,[‡] Frédéric Laquai,[‡] Eric Arifin,[§] Jin-Kyu Lee,[†] Seong Il Yoo,[∥,*] and Byeong-Hyeok Sohn[†,*]

[†]Department of Chemistry, Seoul National University, Seoul, 151-747, Korea, [‡]Max Planck Institute for Polymer Research, Ackermannweg 10, D-55128 Mainz, Germany, [§]Interdisciplinary Program in Nano Science and Technology, NANO System Institute, Seoul National University, Seoul, 151-747, Korea, and [∥]Department of Polymer Engineering, Pukyong National University, Busan 608-739, Korea

ABSTRACT Recently, it has been noticed that surface plasmon resonance of metal nanoparticles can alter the intrinsic properties of nearby fluorophores. Field enhancement and radiative decay engineering are major principles for understanding a number of experimental observations such as enhanced and quenched emission of fluorophores in the vicinity of metal nanoparticles. At the same time, there are apparent similarities between surface-plasmon-coupled fluorescence and fluorescence resonance energy transfer (FRET), as both are near-field through-space interactions. From this perspective, we hypothesize that donor–acceptor interaction in the FRET can be altered by metal nanoparticles. Our approach is based on diblock copolymer micelles, which have been widely applied for nanoscale arrangement of functionalities. By applying self-assembling techniques of copolymer micelles to organize the spatial location of semiconductor quantum dots, fluorescent dyes, and metal nanoparticles, the FRET in hybrid assemblies can be switched off by plasmonic effects.

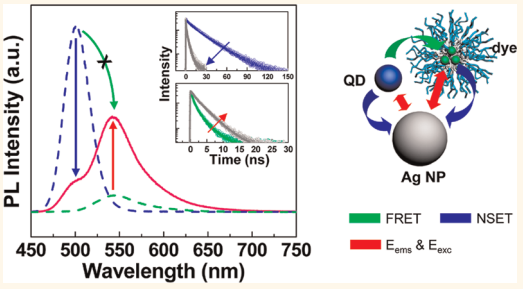

KEYWORDS: self-assembly · micelles · hybrid materials · energy transfer · surface plasmon

Hybridization of dissimilar building materials into highly organized structures can tailor the functionality of each component by coupling phenomena.[1,2] In particular, the collective oscillation of electrons in metal nanoparticles (NPs) known as a localized surface plasmon resonance gained much attention since light–matter interaction can be engineered by positioning metal NPs in the vicinity of fluorophores such as semiconductor quantum dots (QDs) or fluorescent dyes.[3–6] In this context, metal NPs are often referred to as near-field antennas since they can (1) enhance local electric fields around NPs and (2) engineer the radiative and nonradiative decay rate of fluorophores.[3–6] To understand the nature of NP effect, chemically or lithographically fabricated metal NPs and nanostructures have been widely utilized, and it was found that fluorophores in the vicinity of metal NPs undergo excitation enhancement (increased light absorption), emission enhancement (increased radiative decay), or quenching (increased nonradiative decay).[4–15] These competitive near-field interactions arose from several experimental parameters such as the extinction characteristics of metal NPs,[7–9] the distance between NPs and fluorophores,[10–12] and spectral overlap between absorption/emission of fluorophores and the extinction of metal NPs.[13,14] The consequence of those understandings now stimulates widespread applications in biology,[6] diagnostics,[15] photonics,[16] and optoelectronics.[17–19]

These recent findings on plasmonics with metal NPs may highlight the apparent similarity to fluorescence resonance energy transfer (FRET) between a donor–acceptor pair of fluorophores. As well formulated, FRET is a nonradiative through-space energy flow from excited-state donors to ground-state acceptors by dipole–dipole interaction and occurs when the donor-to-acceptor distance is comparable to or smaller than their Förster radius (R_0).[20–25] Therefore, one may envision that donor–acceptor interactions in FRET can be modulated by near-field effects of metal NPs, but such a research direction might be quite complex since multiple parameters aforementioned have to be carefully analyzed. Recently, surface-plasmon-coupled FRET systems have

* Address correspondence to bhsohn@snu.ac.kr, siyoo@pknu.ac.kr.

Received for review February 14, 2012 and accepted May 23, 2012.

Published online May 23, 2012
10.1021/nn301893e

been investigated, however only to a limited degree, using self-assembling techniques such as layer-by-layer assembly[15,26] and multilayered core−shell particles.[27] The pre-existing results suggest that metal NPs can strongly enhance the FRET efficiency by increasing the Förster radius.[28,29] Lakowicz *et al.* inferred that the FRET enhancement might be strongly correlated with a distribution of local electric fields near metal NPs, as such an enhancement was more facilitated with larger metal NPs and shorter distances between NPs and donor−acceptor pairs.[6,28] Considering that the Förster radius is usually in the range 2−6 nm and is too short to be widely applicable for immunoassay of typical globular proteins and antibodies,[6,21] they are convinced that such an enhanced FRET will eventually find an opportunity in biological sensing systems.[6,28]

Another important aspect that needs to be considered is that FRET might also be restricted in the vicinity of metal NPs, and such a restriction may facilitate new material design, as in the case of plasmon-coupled light-emitting diodes (LEDs).[17−19] In a current white LED, for example, multiple fluorophores, which can work as a donor−acceptor pair, are often applied to LED structures to convert high-energy photons to low-energy ones.[30,31] With regard to the lower device performance, one can utilize metal NPs to enhance the spontaneous emission rate and quantum efficiency of emitting materials.[17−19] However, given that the color of LEDs originates from a composition of fluorophores as well as their interaction with metal NPs, the fine-tuning of the emitted color may be quite intricate, unless FRET between multiple fluorophores is restricted.

Perceiving that surface-plasmon-coupled FRET has a fundamental and practical importance in many fields of science, it is important to realize highly organized nano- or meso-structures consisting of metal NPs and fluorophores and to engineer their interactions on a nanometer scale. As a new step in this direction, we report here that FRET in hybrid assemblies of diblock copolymer micelles, QDs, and dyes can be turned off by silver NPs. Our finding strongly suggests that the decay channels of dissimilar fluorophores can be engineered by metal NPs in a way that inhibits FRET. Diblock copolymer micelles were originally selected because (1) a single-layered film of copolymer micelles in a hexagonal order can be easily fabricated by spin-coating,[32−34] (2) some dye molecules are found to be incorporated solely into the core of micelles,[35−37] and (3) QDs can be positioned at the peripheral region of micelles in their single-layered film.[38−40] These unique properties of copolymer micelles discovered by our group and others provide a precise tool for the nanoscale organization of dyes, QDs, and metal NPs to achieve novel material properties and a better understanding of plasmonic effects of metal NPs.

RESULTS AND DISCUSSION

Polystyrene−poly(4-vinylpyridine), PS-PVP, diblock copolymers self-associate into spherical micelles consisting of a soluble PS corona and an insoluble PVP core in toluene, which is a selective solvent for PS blocks.[32,41,42] The molecular weights of PS and PVP blocks in this study are 51 000 and 18 000 g/mol, respectively, with a polydispersity index (PDI) of 1.15 (Polymer Source Inc.). To produce PS-PVP micelles, as-received PS-PVP copolymers were dissolved in toluene (0.5 wt %), stirred for 3 h at 70 °C, and then cooled to room temperature. From the solution, a single-layer film of PS-PVP micelles was fabricated by spin-coating. A transmission electron miscopy (TEM) image (Supporting Information Figure S1) showed spherical micelles arranged in a hexagonal order with a dark PVP core and a bright PS matrix without multilayered structures. The average diameter of PVP cores and the center-to-center distance between micelles were estimated as ∼27 nm and ∼52 nm, respectively. This single-layered film of micelles gives a modality for simultaneous positioning of QDs and dyes that will be described herein.

For a donor−acceptor pair in this study, QDs of core−shell CdSe@ZnS capped by oleic acid were synthesized[43] as a donor, and commercially available rhodamine 123 (R123) was selected as an acceptor. Since the emission/absorption spectra of QDs can be tuned by quantum confinement, one can easily induce the spectral overlap between emission of QD donor and absorption of dye acceptor, which is necessary for FRET studies.[20−25] To produce hybrid assemblies of PS-PVP micelles with QDs and dyes, we first loaded R123 into the PVP core of micelles with a molar ratio of [R123]/[VP] = 0.005. While R123 dyes were not soluble and remained powdery in toluene without micelles, a homogeneous solution was prepared after adding R123 to the micellar solution with vigorous stirring (∼7 days) by a selective inclusion of dyes into the hydrophilic PVP cores.[36,37] The amount of R123 in the PVP core can be controlled by changing the molar ratio of [R123]/[VP], which was confirmed from a gradual change of fluorescence intensity in a dose-dependent manner (see Supporting Information Figure S2). Then, QDs (having a diameter of ∼8.7 nm) were added to the dye-loaded micellar solution (0.3 wt % to the micellar solution). The oleic acid coating on the surface of QDs provided appreciable solubility in toluene and also chemical stability.[43] From the mixture, a single-layered film of micelles with R123 and QDs was prepared by spin-coating (2000 rpm, 60 s), the structure of which was examined by TEM.

In Figure 1a, QDs appear as small dark spots and are distributed around spherical micelles, while PS-PVP micelles are indirectly discernible in the region surrounded by QDs. In addition, PVP cores are recognizable by a gray spherical area in the center of each

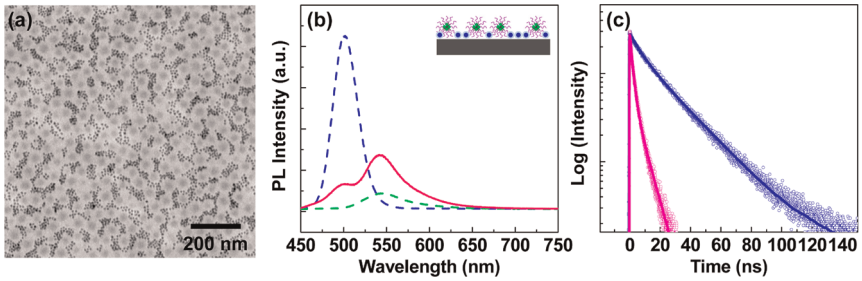

Figure 1. (a) TEM image of a single-layered film of PS-PVP micelles with dyes in the cores and QDs in the periphery. (b) Steady-state fluorescence spectra from micellar film with only QDs (blue dashed line), with only dyes (green dashed line), and with QDs and dyes (pink solid line). (c) Time-resolved fluorescence monitored at 500 nm from micellar film with only QDs (blue) and with QDs and dyes (pink).

micelle even without staining due to their height difference. Noticeably, QDs are mostly located at the peripheral region of PS-PVP micelles without macroscopic separation from them. The center-to-center distance between micelles was increased from 52 to 59 nm by the inclusion of QDs. Since the surface of QDs was functionalized by oleic acid, they were not compatible with the polar PVP core or aromatic PS corona. Therefore, they are physically entrapped between the micelles by a lateral capillary force during the coating process.[38−40] In addition, QDs themselves are separated from each other in a regular spacing (~2.7 nm) without noticeable agglomerations due to the capping agent. While surface modification of QDs by thiol-functionalized polystyrene (PS) can provide compatibility with the PS corona, the PS coating also substantially increases the QD size. From TEM image of Supporting Information Figure S3, PS-coated QDs are found to be macroscopically separated from the micelles presumably because PS-coated QDs are too bulky to occupy the peripheral region of the micelles. With respect to the location of dye molecules, they are most likely located in the PVP cores (gray area in TEM image) because glassy PVP cores cannot be reorganized during the fast spin-coating process.[36,37]

Confirming the fact that both QDs and dyes are simultaneously positioned in the micellar nanostructure, we subsequently focused on the analysis of FRET in the hybrid system with complementary spectroscopic techniques. Prior to that, a single-layered film of micelles with only R123 in the core or micelles with only QDs in the periphery was prepared as a reference. UV−vis and fluorescence spectra from reference samples (Supporting Information Figure S4) showed a strong spectral overlap between QD emission (blue solid line) centered at 500 nm and dye absorption (green dashed line) at 510 nm. In the steady-state fluorescence from micelles with both dyes in the cores and QDs in the periphery (pink solid line in Figure 1b), QD emission at 500 nm was dramatically quenched, while dye emission at 545 nm was enhanced significantly with virtually no shift in the peak position. This indicated an effective energy transfer from the QDs to the dyes in the micellar hybrid. For a comparison, reference fluorescence spectra from micelles containing only QDs (blue dashed line) and micelles containing only R123 (green dashed line) are also included. The excitation wavelength was 442 nm in all cases. FRET was further analyzed by time-resolved fluorescence (TRF) of the QD donor at 500 nm (Figure 1c). Multiexponential fits to the data are included as solid lines to extract some kinetic variables. For micellar films containing only QD donors (blue line), the average lifetime of the donor (τ_D) was 21.8 ns with two decay times of 23.9 ns (87.3%) and 7.0 ns (12.7%). In the case of micelles containing both QD donors and dye acceptors (pink line), the average lifetime of QDs (τ_{DA}) was considerably shortened to 4.30 ns with two rate constants of 1.77 ns (50.3%) and 6.86 ns (49.7%), which confirmed an efficient FRET in the micellar film. From the average lifetime, the FRET rate (k_{FRET}) was calculated to 0.187 ns^{-1} by the relation $k_{FRET} = 1/\tau_{DA} - 1/\tau_D$,[21] and this value will be discussed later.

Having verified FRET in micellar hybrids, it is important to apply the result to metal NP systems to exploit surface-plasmon-coupled FRET. To this end, Ag NPs stabilized by polyvinylpyrrolidone (10 000 g/mol, Sigma-Aldrich) having a 34 nm diameter (Figure 2a) were synthesized as described in the literature.[44] After centrifugation (4000 rpm, 10 min) four times, Ag NPs were redispersed in ethanol at a final concentration of 10 mg mL^{-1}. Then, a film of Ag NPs was fabricated by spin-coating (2000 rpm, 60 s), the extinction of which showed the well-known plasmon resonance at 437 nm (Supporting Information Figure S5). The thickness of the film was about ~1.2 μm, as obtained from the cross-sectional scanning electron microscopy (SEM) image (Figure 2b), but direct visualization of Ag NPs was not possible due to the thick polymer coating on the Ag NPs. Intriguingly, the surface of the Ag film was quite smooth, as shown in the atomic force microscopy (AFM) image (Figure 2c), even if we used Ag NPs of 34 nm diameter. The rms roughness of the film of the Ag NPs was 0.3 nm. Although the Ag NP solution was washed several times, polyvinylpyrrolidone was not completely removed from the solution presumably

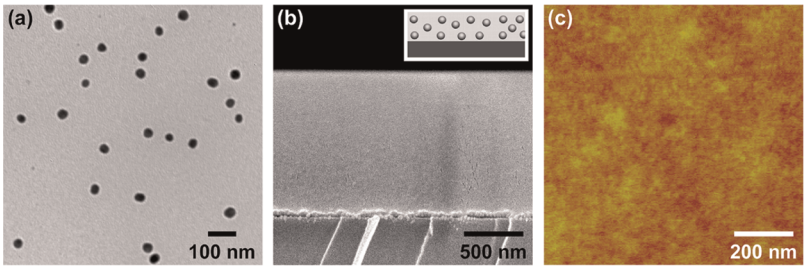

Figure 2. TEM image (a) of Ag NPs and cross-sectional SEM image (b) and AFM image (c) of thin films of Ag NPs.

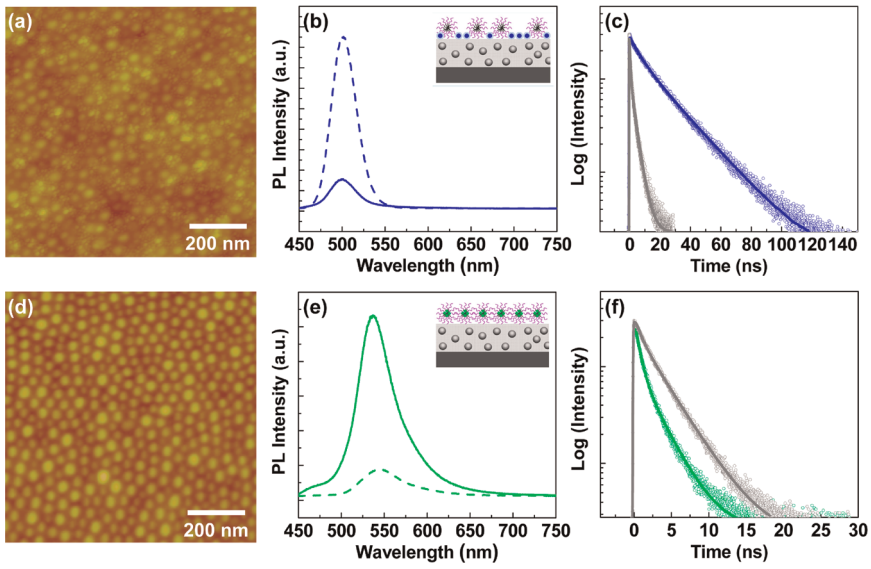

Figure 3. (a, c) AFM images of a single-layered film of PS-PVP micelles with QDs in the periphery (a) and with dyes in the core (c) on the NP film. (b, e) Steady-state fluorescence spectra from a micellar film with QDs in the periphery (b) and with dyes in the core (e). (c, f) Time-resolved fluorescence spectra from a micellar film with QDs in the periphery (c) and with dyes in the core (f). The monitoring wavelengths were 500 and 540 nm for QDs and dyes, respectively.

due to its high viscosity. Hence, the residual polymer may flatten the surface morphology of the Ag films, in turn reducing the surface area.

Given that the surface of the film of Ag NPs (denoted as NP film hereafter) is atomically flat and the solubility of polyvinylpyrrolidone in toluene is negligible (the solubility parameters of toluene and polyvinylpyrrolidone are 18.2, 25.6 $(J/cm^3)^{1/2}$, respectively),[45] we could spin-coat an additional single layer of micelles with dyes in the core or QDs in the periphery directly on the NP film. This allowed us to examine how QDs or dyes can interact with Ag NPs in the micellar film. After coating a single layer of micelles containing only QDs from their mixture, we examined the surface topography by AFM. It should be noted that direct TEM analysis was not possible in this case due to the thick NP film. From AFM, the location of QDs and micelles can be recognized by their size without chemical analysis, as we employed small-sized QDs and large-sized micelles. In Figure 3a, hexagonally ordered micelles are surrounded by QDs with a center-to-center distance between micelles of 61 nm. This value was found to be virtually identical to that (59 nm) of the bare substrate. However, a sharp visualization of QDs was hindered in the AFM analysis, which further indicates that QDs are most likely located on the surface of the NP film with an appreciable overlap with the PS corona.

With this structural information, we focused on the NP effect on the fluorescence of QDs. In the steady-state fluorescence (Figure 3b), the QD emission at 500 nm on a bare substrate (dashed line) became strongly quenched when the same micellar film was coated on the NP film (solid line). To gain further insights into the NP effect, TRF of QDs was monitored at 500 nm in the absence and presence of NP films. In Figure 3c, the blue fitting curve was obtained from micelles with QDs on a bare substrate, which showed an average lifetime of 21.8 ns, having two components of 23.9 ns (87.3%) and 7.0 ns (12.7%). When the same micellar film was coated on the NP film (gray line), the decay process of QDs became much faster, with an average lifetime of 2.57 ns, having two decay components of 3.16 ns (77.9%) and 0.50 ns (22.1%). In general, the lifetime of fluorophores is inversely proportional to the total decay rate (k_t^0), which is the sum of the radiative decay rate (k_{rad}^0) and the nonradiative decay rate (k_{nr}^0).[21] On the other hand, if fluorophores are placed in the vicinity of metal NPs, surface plasmons

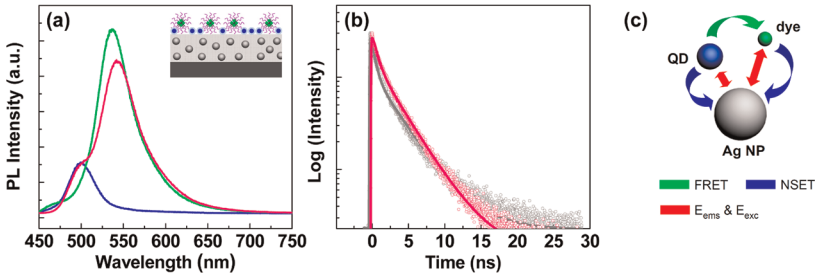

Figure 4. (a) Steady-state fluorescence spectra from a single-layered film of micelles on a NP film with only QDs (blue), with only dyes (green), and with QDs and dyes (pink). (b) Time-resolved fluorescence monitored at 500 nm from a single-layered film of micelles on the NPs film with only QDs (pink) and with QDs and dyes (gray). Multiexponential fits were included as solid lines. (c) Schematics of near-field interactions among QDs, dyes, and Ag NPs in the micellar hybrid. Green, blue, and red arrows were used for presenting FRET, NSET, and excitation/emission enhancement factors, respectively.

of metal NPs can affect the intrinsic radiative and nonradiative decay rate of fluorophores.[4,6,46−48] Therefore, the shortened lifetime illustrated by a steeper slope in the TRF of QDs indicates that either k^0_{rad} or k^0_{nr} was increased by the NP film. However, the radiative decay rate cannot be increased in this case, as we observed quenched QD emission in Figure 3b. Therefore, the shortened lifetime of QDs on the NP film can be attributed to an increased nonradiative decay rate by metal NPs. This quenched QD emission may be comparable to a recent study by Mahrt and co-workers.[49] In their paper, they incorporated dye molecules and small Ag NPs (2−3 nm) simultaneously into the PVP core of PS-PVP micelles. As a result, the fluorescence of the dyes was quenched with a shortened lifetime by the closeness of the dyes to the NPs, which was explained by a nonradiative energy transfer process.

Subsequently, we spin-coated micelles containing dyes in the cores on the NP film. An AFM image showed a hexagonal array of spherical micelles with a center-to-center distance of 52 nm (Figure 3d), similar to those on a bare substrate. However, quite different results were obtained from the fluorescence data in the absence and presence of the NP film. Clearly, the dye emission at 545 nm on a bare substrate (dashed line in Figure 3e) was greatly enhanced after coating the same structure on the NP film (solid line). In addition, the peak position was blue-shifted from 545 to 537 nm. Therefore, one can speculate that the NPs exerted a different effect on QDs and dyes in micellar films. TRFs of dyes on a bare substrate (green line) and on the NP film (gray line) were also monitored at 540 nm (Figure 3f). The decay profile of dyes on a bare substrate showed an average lifetime of 1.96 ns with two decay components of 2.70 ns (64.2%) and 0.62 ns (35.8%). Since the dye molecules in a dilute ethanol solution showed a single-exponential decay with a lifetime of 3.89 ns (Supporting Information Figure S6), the short component of 0.62 ns can be attributed to some agglomeration of dye molecules in the PVP cores. When the same micelles were coated on the NP film, the average lifetime of the dyes was increased to 3.17 ns with two decay components of 3.42 ns (90.7%) and 0.75 ns (9.3%). This increased lifetime apparently contradicts the general NP effect discussed before. In order to enhance dye emission, the intrinsic radiative decay rate of the dyes has to be increased, and therefore the lifetime of the dyes has to be reduced. The abnormality observed here can be attributed to the dye agglomeration in the micellar core. Note, such an agglomeration usually red-shifts the fluorescence peak position and also reduces the lifetime by a self-quenching mechanism.[21] Therefore, the NP effect on the dye molecules can be understood as reduction of the self-quenching process. This feature can explain a number of observations: (a) an increased lifetime of the dyes along with a reduced amplitude of the short time component in TRF and (b) the blue-shifted steady-state fluorescence of dyes on the NP films. As we noted that this kind of NP effect has not been reported yet, a systematic study of the NP effect on the self-quenching process will follow in future work.

On the basis of the information collected so far, we decided to coat a single-layered film of micelles with both dyes in a core and QDs in the periphery on the NP film (denoted by micelles with QD/dye/NP hereafter). It is important to recall that the same micellar film on a bare substrate showed efficient FRET from QD donors to dye acceptors in Figure 1. In stark contrast, when the same micelles containing both dyes and QDs were applied to the NP film, the fluorescence spectrum from QDs at 500 nm and dyes at 545 nm basically remained unaltered (pink line in Figure 4a) compared to the fluorescence spectra from micelles containing only QDs (blue line) and micelles containing only dyes (green line) on the NP film, *i.e.*, the quenched QD emission and enhanced dye emission on the NPs film discussed in Figure 3. The slight decrease in the dye emission at 545 nm can be attributed to the reduced number of micelles because QDs replaced some of the micelles in the mixed film. Furthermore, the average lifetime and fluorescence time components of the QD donors were greatly maintained, even in the presence of dye acceptors when they were placed on the NP film (see TRF in Figure 4b). In other words, *Ag NPs completely switched off FRET from QDs to dyes in a micellar hybrid*. From the decay profile of the QD donors from micelles with QD/dye/NP (gray line) an average lifetime

of 2.84 ns with two decay times of 3.33 ns (81.9%) and 0.64 ns (18.1%) was extracted. These values were nearly identical to those obtained from micelles with only QDs on the NP films (pink line), which have an average lifetime of 2.57 ns with two decay times of 3.16 ns (77.9%) and 0.50 ns (22.1%). The inhibited FRET by Ag NPs was further confirmed by comparing TRF spectra of dye acceptors at 540 nm. When micelles with QDs and dyes were coated on a bare substrate, time-dependent intensity of dye fluorescence was increased with a rise component of 0.59 ns (Supporting Information Figure S7a). However, when the same micellar film was coated on the NP film, no rise component was detected in the TRF spectrum (Supporting Information Figure S7b). Since the rise component is an indication of additional excitation of dyes by energy transfer from QDs, it further confirms that FRET was inhibited by Ag NPs in the micellar hybrid.

How can FRET in micellar films be switched off by metal NPs? In order to answer this question, one has to consider all the near-field interactions among QDs, dyes, and Ag NPs in their hybrid structures. At the beginning, it would be instructive to discuss general aspects of NP effects on nearby fluorophores and to quantitatively analyze the spectroscopic results in Figures 3 and 4 according to recent kinetic models.[4,6,46−48,50,51] In general, the emission rate of fluorophores can be described as $\gamma^0_{exc}Q^0$, where γ^0_{exc} is the excitation rate and Q^0 is the quantum yield of the fluorophores. Metal NPs can potentially affect the intrinsic excitation rate and quantum yield with the following processes. In the micellar hybrid of Figure 4, as the extinction spectrum of the NP film is centered at 437 nm, the incident light (442 nm) excites the surface plasmon of Ag NPs, which subsequently creates a strong electromagnetic field. Thus, the excitation rate of QDs or dyes in the vicinity of Ag NPs can be enhanced. In addition, the excited fluorophores further induce an electron oscillation in the Ag NPs and lead to resonance between fluorophores and Ag NPs. This coupling effect can affect the quantum yield of fluorophores by modifying the intrinsic radiative (k^0_{rad}) and nonradiative decay (k^0_{nr}) rate with k_{rad} and k_{nr}, respectively. At the same time, the excited-state energy of fluorophores can be transferred to metal NPs and then dissipated as heat. This nonradiative energy transfer to metal NPs is inversely proportional to the fourth power of the distance between the fluorophores and the surface of metal NPs and can be adequately described by the empirical nanometal surface energy transfer (NSET) mechanism.[50,51] Perceiving that QDs are stabilized by oleic acid and dyes are located in the PVP cores that are surrounded by PS coronas, the separation of QDs and dyes from the surface of Ag NPs can be evaluated from the thickness of stabilizers or PS coronas. Within this structural picture, the NSET efficiency was calculated as 0.99 for QDs and 0.08 for dyes in the micellar films, respectively. (see Supporting Information). The proximity of the QDs to the NP film facilitated the NSET process, while such a process is restricted to dyes in the PVP core due to the large separation by the PS coronas.

By combining the aforementioned near-field interactions, the overall NP effect on the nearby fluorophores can be expressed as the total enhancement factor (E), which is a product of the excitation enhancement factor (E_{exc}) and the emission enhancement factor (E_{ems}) originating from the modified excitation rate and the decay rate by metal NPs.[4,6,13,46−48] Experimentally, the total enhancement factor can be determined from the intensity ratio of the steady-state fluorescence from bare substrates and from the NP film in Figure 3. Then, the total enhancement factor can be further resolved into the excitation enhancement factor (E_{exc}) and the emission enhancement factor (E_{ems}) by the TRF spectra in Figure 3. By combining these enhancement factors with the lifetime information, all the decay rates (k^0_{rad}, k^0_{nr}, k_{rad}, k_{nr}, and k_{NSET}) can be determined, which are summarized in the Supporting Information Table S2 (this is discussed in greater detail in the Supporting Information).

All these considerations can provide a rationale on the inhibited FRET presented in Figure 4a and b. At the beginning, we considered all the near-field interactions among QDs, dyes, and NPs as depicted in Figure 4c. In the schematics, FRET, NSET, and excitation/emission enhancement factors are represented by green, blue, and red arrows, respectively. However, the excitation enhancement factor (E_{exc}) cannot change the intrinsic radiative and nonradiative decay processes that are occurring after excitation, and so this factor can be excluded in the discussion of inhibited FRET. The emission enhancement factor (E_{ems}) indeed altered the intrinsic decay processes, and this effect was taken into consideration as k_{rad} and k_{nr}. Furthermore, the NSET process from dyes to metal NPs can be neglected by the thick PS coronas, as we have already discussed. Therefore, after excluding the aforementioned interactions, the question of how the FRET from QDs to dyes was inhibited by metal NPs can be rephrased as, which decay process is the more favorable one for the excited QDs. In other words, there is a competition among radiative decay, nonradiative decay, FRET, and NSET processes for the excited QDs in the hybrid structure. Since the rate constants of radiative (k_{rad}), nonradiative (k_{nr}), and NSET (k_{NSET}) processes in the presence of metal NPs were calculated as 0.009, 0.008, and 0.373 ns^{-1} (Supporting Information), respectively, and the FRET rate (k_{FRET}) was evaluated as 0.187 ns^{-1} in Figure 1, one can see the nonradiative energy transfer to Ag NPs (NSET) is much faster than all the other decay processes. All together, these features allow the donor (QDs)−acceptor (dyes) interaction in FRET to be turned off by metal NPs in the micellar hybrid.

Considering the fastest NSET process was created by the closeness of QDs to the NP film, it can also be blocked by introducing a spacer layer that alienates QDs from the NP film. To test this idea, a spacer layer of poly(2-vinlyprindine) (P2VP) homopolymer of 15.5 nm thickness was inserted between the NP film and the micellar film. In such a hybrid structure, it turns out that the NSET process becomes insignificant and FRET becomes the fastest decay processes for the excited QDs. As a result, FRET from QDs to dyes can be retrieved even in the presence of the NP film (see Supporting Information Figure S9).

CONCLUSION

Our results strongly suggest that near-field interactions among QDs, dyes, and metal NPs can be engineered by nanoscale organization. Both the radiative and nonradiative decay processes of fluorophores were controlled in the vicinity of metal NPs to induce either enhanced or quenched fluorescence. In particular, FRET from QDs to dyes was inhibited by the presence of metal NPs, which was explained by the fastest NSET decay process by the closeness of QDs and metal NPs. In addition, after introducing a spacer layer of P2VP homopolymer, the inhibited FRET can be retrieved even in the presence of the NP film. One can assess the prospects of this result from a perspective of turning on and off FRET by NP–fluorophore interactions. In this regard, metal NPs can be considered as an optical switch, which can potentially control FRET in optoelectric devices or in biological systems such as fluorophore-labeled proteins. Overall, a number of features discussed in this study can stimulate future interest in plasmonic effects on hybrid systems and also represent a new approach for engineering mutual interactions between dissimilar functionalities in the framework of block copolymers. Systematic tuning of the extinction spectrum of metal NPs may help create a better understanding of the underlying physical process and can be suggested as a future direction.

EXPERIMENTAL SECTION

Polystyrene–poly(4-vinylpyridine) was purchased from Polymer Source, Inc. The number average molecular weights of PS and PVP blocks are 51 000 and 18 000 g/mol, respectively, with a PDI of 1.15. PS-PVP copolymers were dissolved in toluene (0.5 wt %) at room temperature, heated to 70 °C for 3 h, and then cooled to room temperature with mild stirring. Rhodamine 123 (Sigma-Aldrich) was added to a toluene solution of PS-PVP micelles with a molar ratio of [R123]/[VP] = 0.005, and then the solution was vigorously stirred for at least 7 days for a selective inclusion of R123 into the PVP cores. QDs of core–shell CdSe@ZnS capped by oleic acid were synthesized as in the literature and then dried under vacuum.[43] Then, QDs in a powdery state were dissolved in the micellar solution (weight percent of QDs in micellar solution was 0.3 wt %). A single-layered film of PS-PVP micelles with and without dyes or QDs was prepared by spin-coating (2000 rpm, 60 s).

To synthesize polyvinylpyrrolidone-stabilized Ag NPs, 10 g of polyvinylpyrrolidone (10 000 g/mol, Sigma-Aldrich) was dissolved in 50 mL of ethylene glycol at room temperature. Then, 800 mg of silver nitrate was added to the ethylene glycol solution. The reaction mixture was heated to 120 °C under stirring for 1 h to reduce silver nitrate to Ag NPs.[44] To purify Ag NPs, an excess amount of acetone was added to the NP solution and the solution was centrifuged at 4000 rpm for 10 min. After carefully removing the supernatant, the precipitates were redispersed in ethanol. This process was repeated four times. The final concentration of Ag NPs in ethanol was adjusted as 10 mg/mL, which was used for spin-coating on quartz plates or Si-wafers (2000 rpm, 60 s). Before coating, the substrates were cleaned in a piranha solution (70/30 v/v of concentrated H_2SO_4 and 30% H_2O_2).

UV–vis absorption spectra were recorded on a Varian Cary-5000 spectrophotometer. Steady-state fluorescence was measured on an Acton SpectraPro with a He–Cd laser (442 nm) as the excitation source. Time-resolved fluorescence was obtained using the time-correlated single-photon counting (TCSPC) technique. The excitation source is a self-mode-locked femtosecond Ti:Sapphire laser (Coherent model Mira 900) pumped by an Nd:YVO_4 laser (Coherent Verdi diode-pumped laser). The laser output has a pulse width of ~260 fs and can span excitation wavelengths in the range 350–490 nm by second-harmonic generation. The excitation wavelength was 420 nm. All the standard electronics for the TCSPC system were from Edinburgh Instruments, which provided a temporal resolution less than 10 ps after deconvolution of instrument response function. This picosecond setup can measure the decay and the rise of fluorescence after laser pulse excitation.[52,53] All measurements were performed at room temperature. Surface morphologies of thin films of Ag NPs and hybrid assemblies of PS-PVP micelles, QDs, and dyes were investigated by atomic force microscopy (AFM Nanoscope IIIA, Digital Instrument) in tapping mode with Si cantilevers. The morphology of the nanoparticles and single-layered films of micelles was investigated by transmission electron microscopy (Hitachi 7600) and field-emission scanning electron microscopy (JSM-6700F JEOL) after Pt coating on the sample.

Conflict of Interest: The authors declare no competing financial interest.

Acknowledgment. This work was supported by the Mid-Career Researcher Program of the National Research Foundation of Korea (NRF) funded by the Ministry of Education, Science, and Technology (MEST) (No. 2012-0005319). S.I.Y. acknowledges the support by Basic Science Research Program through the National Research Foundation of Korea (NRF) funded by the Ministry of Education, Science and Technology (2012R1A1A1001453).

Supporting Information Available: Additional information and figures. This material is available free of charge *via* the Internet at http://pubs.acs.org.

REFERENCES AND NOTES

1. Nie, Z.; Petukhova, A.; Kumacheva, E. Properties and Emerging Applications of Self-Assembled Structures Made from Inorganic Nanoparticles. *Nat. Nanotechnol.* **2010**, *5*, 15–25.
2. Lee, J.; Hernandez, P.; Lee, J.; Govorov, A. O.; Kotov, N. A. Exciton-Plasmon Interactions in Molecular Spring Assemblies of Nanowires and Wavelength-Based Protein Detection. *Nat. Mater.* **2007**, *6*, 291–295.
3. Novotny, L.; Hulst, N. V. Antennas for Light. *Nat. Photonics* **2011**, *5*, 83–90.
4. Giannini, V.; Fernández-Domíguez, A. I.; Heck, S. C.; Maier, S. A. Plasmonic Nanoantennas: Fundamentals and Their Use in Controlling the Radiative Properties of Nanoemitters. *Chem. Rev.* **2011**, *111*, 3888–3912.
5. Kinkhabwala, A.; Yu, Z.; Fan, S.; Avlasevich, Y.; Müllen, K.; Moerner, W. E. Large Single-Molecule Fluorescence

Enhancements Produced by a Bowtie Nanoantenna. *Nat. Photonics* **2009**, *3*, 654–657.
6. Lakowicz, J. R.; Ray, K.; Chowdhury, M.; Szmacinski, H.; Fu, Y.; Zhang, J.; Nowaczyk, K. Plasmon-Controlled Fluorescence: A New Paradigm in Fluorescence Spectroscopy. *Analyst* **2008**, *133*, 1308–1346.
7. Rycenga, M.; Cobley, C. M.; Zeng, J.; Li, W.; Moran, C. H.; Zhang, Q.; Qin, D.; Xia, Y. Controlling the Synthesis and Assembly of Silver Nanostructures for Plasmonic Applications. *Chem. Rev.* **2011**, *111*, 3669–3712.
8. Bardhan, R.; Grady, N. K.; Cole, J. R.; Joshi, A.; Halas, N. J. Fluorescence Enhancement by Au Nanostructures: Nanoshells and Nanorods. *ACS Nano* **2009**, *3*, 744–752.
9. Tam, F.; Goodrich, G. P.; Johnson, B. R.; Halas, N. J. Plasmonic Enhancement of Molecular Fluorescence. *Nano Lett.* **2007**, *7*, 496–501.
10. Ratchford, D.; Shafiei, F.; Kim, S.; Gray, S. K.; Li., X. Manipulating Coupling between a Single Semiconductor Quantum Dot and Single Gold Nanoparticle. *Nano Lett.* **2011**, *11*, 1049–1054.
11. Ray, K.; Badugu, R.; Lakowicz, J. R. Polyelectrolyte Layer-by-Layer Assembly to Control the Distance between Fluorophores and Plasmonic Nanostructures. *Chem. Mater.* **2007**, *19*, 5902–5909.
12. Schneider, G.; Decher, G.; Nerambourg, N.; Praho, R.; Werts, M. H. V.; Blanchard-Desce, M. Distance-Dependent Fluorescence Quenching on Gold Nanoparticles Ensheathed with Layer-by-Layer Assembled Polyelectrolytes. *Nano Lett.* **2006**, *6*, 530–536.
13. Munechika, K.; Chen, Y.; Tillack, A. F.; Kulkarni, A. P.; Plante, I. J. L.; Munro, A. M.; Ginger, D. S. Spectral Control of Plasmonic Emission Enhancement from Quantum Dots near Single Silver Nanoprisms. *Nano Lett.* **2010**, *10*, 2598–2603.
14. Chem, Y.; Munechika, K.; Ginger, D. S. Dependence of Fluorescence Intensity on the Spectral Overlap between Fluorophores and Plasmon Resonant Single Silver Nanoparticles. *Nano Lett.* **2007**, *7*, 690–696.
15. Wang, Y.; Liu, B.; Mikhailovsky, A.; Bazan, G. C. Conjugated Polyelectrolyte-Metal Nanoparticle Platforms for Optically Amplified DNA Detection. *Adv. Mater.* **2010**, *22*, 656–659.
16. Noginovl, M. A.; Zhul, G.; Belgravel, A. M.; Bakker, R.; Shalaev, V. M.; Narimanov, E. E.; Stoutl, S.; Herz, E.; Suteewong, T.; Wiesner, U. Demonstration of a Spaser-Based Nanolaser. *Nature* **2009**, *460*, 1110–1113.
17. Kim, T. H.; Cho, K. S.; Lee, E. K.; Lee, S. J.; Chae, J.; Kim, J. W.; Kim, D. H.; Kwon, J. Y.; Amaratunga, G.; Lee, S. Y.; *et al.* Full-Colour Quantum Dot Displays Fabricated by Transfer Printing. *Nat. Photonics* **2011**, *5*, 176–182.
18. Kwon, M. K.; Kim, J. Y.; Kim, B. H.; Park, I. K.; Cho, C. Y.; Byeon, C. C.; Park, S. J. Surface-Plasmon-Enhanced Light-Emitting Diodes. *Adv. Mater.* **2008**, *20*, 1253–1257.
19. Ozbay, E. Plasmonics: Merging Photonics and Electronics at Nanoscale Dimensions. *Science* **2006**, *311*, 189–193.
20. Sapsford, K. E.; Berti, L.; Medintz, I. L. Materials for Fluorescence Resonance Energy Transfer Analysis: Beyond Traditional Donor-Acceptor Combinations. *Angew. Chem., Int. Ed.* **2006**, *45*, 4562–4588.
21. Lakowicz, J. R. *Principles of Fluorescence Spectroscopy*, 3rd ed.; Kluwer Academic/Plenum Publishers: New York, 2006; pp 443−475.
22. Yoo, S. I.; Bae, S. H.; Kim, K. S.; Sohn, B.-H. Nanostructures of Diblock Copolymer Micelles for Controlled Fluorescence Resonance Energy Transfer. *Soft Matter* **2009**, *5*, 2990–2996.
23. Reil, F.; Hohenester, U.; Krenn, J. R.; Leitner, A. Förster-Type Resonant Energy Transfer Influenced by Metal Nanoparticles. *Nano Lett.* **2008**, *12*, 4128–4133.
24. Medintz, I. L.; Uyeda, H. T.; Goldman, E. R.; Mattoussi, H. Quantum Dot Bioconjugates for Imaging, Labeling and Sensing. *Nat. Mater.* **2005**, *4*, 435–446.
25. Jares-Erijman, E. A.; Jovin, T. M. FRET Imaging. *Nat. Biotechnol.* **2003**, *21*, 1387–1395.
26. Lunz, M.; Gerard, V. A.; Gun'ko, Y. K.; Lesnyak, V.; Gaponik, N.; Susha, A. S.; Rogach, A. L.; Bradley, A. L. Surface Plasmon Enhanced Energy Transfer between Donor and Acceptor CdTe Nanocrystal Quantum Dot Monolayers. *Nano Lett.* **2011**, *11*, 3341–3345.
27. Lessard-Viger, M.; Rioux, M.; Rainville, L.; Boudreau, D. FRET Enhancement in Multilayer Core-Shell Nanoparticles. *Nano Lett.* **2009**, *9*, 3066–3071.
28. Zhang, J.; Fu, Y.; Chowhury, M. H.; Lakowicz, J. R. Enhanced Förster Resonance Energy Transfer on Single Metal Particle. 2. Dependence on Donor-Acceptor Separation Distance, Particle Size, and Distance from Metal Surface. *J. Phys. Chem. C* **2007**, *111*, 11784–11792.
29. Van Duyne, R. P. Molecular Plasmonics. *Science* **2004**, *306*, 985–986.
30. Achermann, M.; Petruska, M. A.; Koleske, D. D.; Crawford, M. H.; Klimov, V. I. Nanocrystal-Based Light-Emitting Diodes Utilizing High-Efficiency Nonradiative Energy Transfer for Color Conversion. *Nano Lett.* **2006**, *6*, 1396–1400.
31. Achermann, M.; Petruska, M. A.; Kos, S.; Smith, D. L.; Koleske, D. D.; Klimov, V. I. Energy-Transfer Pumping of Semiconductor Nanocrystals Using an Epitaxial Quantum Well. *Nature* **2004**, *429*, 642–646.
32. Yoo, S. I.; Kwon, J. H.; Sohn, B. H. Single Layers of Diblock Copolymer Micelles for the Fabrication of Arrays of Nanoparticles. *J. Mater. Chem.* **2007**, *17*, 2969–2975.
33. Aizawa, M.; Buriak, J. M. Block Copolymer Templated Chemistry for the Formation of Metallic Nanoparticle Arrays on Semiconductor Surfaces. *Chem. Mater.* **2007**, *19*, 5090–5101.
34. Glass, R.; Möller, M.; Spatz, J. P. Block Copolymer Micelle Nanolithography. *Nanotechnology* **2003**, *14*, 1153–1160.
35. Rainò, G.; Stöferle, T.; Park, C.; Kim, H. C.; Chin, I. J.; Miller, R. D.; Mahrt, R. F. Dye Molecules Encapsulated in a Micelle Structure: Nano-Aggregates with Enhanced Optical Properties. *Adv. Mater.* **2010**, *22*, 3681–3684.
36. Yoo, S. I.; Lee, J. H.; Sohn, B. H.; Eom, I.; Joo, T.; An, S. J.; Yi, G.-C. Enhancement and Concurrence of Emissions from Multiple Fluorophores in a Single Emitting Layer of Micellar Nanostructures. *Adv. Funct. Mater.* **2008**, *18*, 2984–2989.
37. Yoo, S. I.; An, S. J.; Choi, G. H.; Kim, K. S.; Yi, G.-C.; Zin, W.-C.; Jung, J. C.; Sohn, B. H. Controlled Light Emission by Nanoencapsulation of Fluorophores in Thin Films of Diblock Copolymer Micelles. *Adv. Mater.* **2007**, *19*, 1594–1596.
38. Acharya, H.; Sung, J.; Sohn, B. H.; Kim, D. H.; Tamada, K.; Park, C. Tunable Surface Plasmon Band of Position Selective Ag and Au Nanoparticles in Thin Block Copolymer Micelle Films. *Chem. Mater.* **2009**, *21*, 4248–4255.
39. Bae, S. H.; Yoo, S. I.; Bae, W. K.; Lee, S.; Lee, J. K.; Sohn, B. H. Single-Layered Films of Diblock Copolymer Micelles Containing Quantum Dots and Fluorescent Dyes and Their Fluorescence Resonance Energy Transfer. *Chem. Mater.* **2008**, *20*, 4185–4187.
40. Sohn, B. H.; Choi, J. M.; Yoo, S. I.; Yoon, S. H.; Zin, W.-C.; Jung, J. C.; Kanehara, M.; Hirata, T.; Teranishi, T. Directed Self-Assembly of Two Kinds of Nanoparticles Utilizing Monolayer Films of Diblock Copolymer Micelles. *J. Am. Chem. Soc.* **2003**, *125*, 6368–6369.
41. Lohmueller, T.; Bock, E.; Spatz, J. P. Synthesis of Quasi-Hexagonal Ordered Arrays of Metallic Nanoparticles with Tuneable Particle Size. *Adv. Mater.* **2008**, *20*, 2297–2302.
42. Förster, S.; Antonietti, M. Amphiphilic Block Copolymers in Structure-Controlled Nanomaterial Hybrids. *Adv. Mater.* **1998**, *10*, 195–217.
43. Bae, W. K.; Kwak, J.; Park, J. W.; Char, K.; Lee, C.; Lee, S. Highly Efficient Green-Light-Emitting Diodes Based on CdSe@ZnS Quantum Dots with a Chemical-Composition Gradient. *Adv. Mater.* **2009**, *21*, 1690–1694.
44. Silvert, P.-Y.; Herrer-Urbina, R.; Duvauchelle, N.; Vijayakrishnan, V.; Tekaia-Elhsissen, K. Preparation of Colloidal Silver Dispersions by the Polyol Process Part 1-Synthesis and Characterization. *J. Mater. Chem.* **1996**, *6*, 573–577.
45. Brandrup, J.; Immergut, E. H.; Grulke, E. A., Eds. *Polymer Handbook*, 4th ed.; Wiley-Interscience: New York, 1999.

46. Govorov, A. O.; Bryant, G. W.; Zhang, W.; Skeini, T.; Lee, J.; Kotov, N. A.; Slocik, J. M.; Naik, R. R. Exciton-Plasmon Interaction and Hybrid Excitons in Semiconductor-Metal Nanoparticle Assemblies. *Nano Lett.* **2006**, *6*, 984–994.
47. Dulkeith, E.; Ringler, M.; Klar, T. A.; Feldmann, J. Gold Nanoparticles Quench Fluorescence by Phase Induced Radiative Rate Suppression. *Nano Lett.* **2005**, *5*, 585–589.
48. Dulkeith, E.; Morteani, A. C.; Niedereichholz, T.; Klar, T. A.; Feldmann, J.; Levi, S. A.; van Veggel, F. C. J. M.; Reinhoudt, d. N.; Möller, M.; Gittins, D. I. Fluorescence Quenching of Dye Molecules near Gold Nanoparticles: Radiative and Nonradiative Effects. *Phys. Rev. Lett.* **2002**, *89*, 203002.
49. Rainò, G.; Stöferle, T.; Park, C.; Kim, H.-C.; Topuria, T.; Rice, P. M.; Chin, I.-J.; Miller, R. D.; Mahrt, R. F. Plasmonic Nanohybrid with Ultrasmall Ag Nanoparticles and Fluorescent Dyes. *ACS Nano* **2011**, *5*, 3536–3541.
50. Singh, M. P.; Strouse, G. F. Involvement of the LSPR Spectral Overlap for Energy Transfer between a Dye and Au Nanoparticle. *J. Am. Chem. Soc.* **2010**, *132*, 9383–9391.
51. Jennings, T. L.; Singh, M. P.; Strouse, G. F. Fluorescent Lifetime Quenching near d=1.5 nm Gold Nanoparticles: Probing NSET Validity. *J. Am. Chem. Soc.* **2006**, *128*, 5462–5467.
52. Soujon, D.; Becker, K.; Rogach, A. L.; Feldman, J.; Weller, H.; Talapin, D. V.; Lupton, J. M. Time-Resolved Föster Energy Transfer from Individual Semiconductor Nanoantennae to Single Dye Molecules. *J. Phys. Chem. C* **2007**, *111*, 11511–11515.
53. De Schryver, F. C.; Vosch, T.; Cotlet, M.; Van Der Auweraer, M.; Müllen, K.; Hofkens, J. Energy Dissipation in Multichromophoric Single Dendrimers. *Acc. Chem. Res.* **2005**, *38*, 514–522.